Pt/carbon materials as bi-functional catalysts for *n*-decane hydroisomerization

Sara Fernandes[a], Marta Andrade[a], Conchi O. Ania[b] Angela Martins[c,*], João Pires[a], Ana P. Carvalho[a,*]

[a] Universidade de Lisboa, Faculdade de Ciências, Departamento de Química e Bioquímica and CQB, Campo Grande C8, 1749-016 Lisboa, Portugal

[b] Dpt. Chemical Processes in Energy and Environment Instituto Nacional del Carbón (INCAR, CSIC), Apdo. 73, 33011 Oviedo (Spain)

[c] Instituto Superior de Engenharia de Lisboa, Departamento de Engenharia Química and CIEQB, R. Conselheiro Emídio Navarro, 1959-007 Lisboa, Portugal

Activated carbons are widely used as adsorbents,

[1-4].Activated carbons are widely used as adsorbents,

*Corresponding Authors: Angela Martins, Departamento de Engenharia Química and CIEQB, Instituto Superior de Engenharia de Lisboa, R. Conselheiro Emídio Navarro, 1959-007 Lisboa, Portugal; Tel: +351 218317000; Fax: +351 218317001; *E-mail address*: amartins@deq.isel.ipl.pt; Ana P. Carvalho; Faculdade de Ciências da Universidade de Lisboa, Campo Grande C8, 1749-016 Lisboa, Portugal; Tel.: +351 217500897; Fax: +351 217500088; *E-mail address:* ana.carvalho@fc.ul.pt.

Abstract

The activity and selectivity of bi-functional carbon-supported platinum catalysts for the hydroisomerization of *n*-alkanes have been studied. The influence of the properties of the carbon support on the performance of the catalysts were investigated by incorporating the metallic function on a series of carbons with varied porosity (microporous: GL-50 from Norit, and mesoporous: CMK-3) and surface chemistry (modified by wet oxidation). The characterization results achieved with H_2 chemisorption and TEM showed differences in surface metal concentrations and metal–support interactions depending on the support composition. The highest metal dispersion was achieved after oxidation of the carbon matrix in concentrated nitric acid, suggesting that the presence of surface functional sites distributed in inner and outer surface favours a homogeneous metal distribution. On the other hand, the higher hydrogenating activity of the catalysts prepared with the mesoporous carbon pointed out that a fast molecular traffic inside the pores plays an important role in the catalysts performance. For *n*-decane hydroisomerization of long chain *n*-alkanes, higher activities were obtained for the catalysts with an optimized acidity and metal dispersion along with adequate porosity, pointing out the importance of the support properties in the performance of the catalysts.

Keywords:

Bifunctional catalysts; Activated carbons; Ordered mesoporous carbon CMK-3; Acidity; Platinum; *n*-decane hydroisomerization

1. Introduction

Activated carbons are amorphous materials with unique properties due to their large internal surface area, pore volume and surface chemistry properties, which have been extensively used in many science and engineering fields as adsorbents, catalysts and catalysts supports [1-4]. The majority of these applications derives from the flexible coordination chemistry of carbon atoms that allows an infinite possibility of three-dimensional structures with expanded pore network, and their versatile surface chemistry [1, 5, 6]. This ability of carbons to control their physicochemical features by selecting an adequate precursor and/or incorporating surface functionalities (self-organization, chemical stability, reactivity), provides a useful and unlimited tool to design carbon materials and to control and modulate its performance in a specific application.

The relatively high inertness of activated carbons surfaces and their stability in highly acidic and basic media are other important properties that allow their widespread use in catalytic applications. The severity of reaction conditions (in terms of pressure and temperature) needed in some processes, such as hydrogenation, makes carbon materials most suitable supports compared to silica or alumina-based materials [7]. In this sense, despite the abundance of studies on the preparation and use of carbon-supported metallic catalysts (for instance, Ru, Pd, Mo, Ni and Pt), there is still some lack of consensus on the effect of the textural features and chemical composition of the carbon support on the metal dispersion and the latter activity of the catalyst. [8-12]. One of the main cornerstones in the design of supported catalysts is to obtain a high dispersion of the catalytically active phase (i.e., the metallic function) on the support while maintaining an open porous structure of the catalyst to avoid diffusion constrains to the

reagents or products. A further advantage can be gained if a suitable interaction between the metallic function and the support is achieved. In this regard, the broad pore size distribution of the majority of activated carbons, comprised of narrow micropores, becomes a drawback due to the small size of the pores to accommodate the metal particles of appropriate size, which in many cases results in poor catalytic performance of the catalysts [8]. The use of nanostructured carbon materials showing a wide porous network represents a good option to overcome this problem, increasing the dispersion of the metallic phase and minimizing metal dislodgement and/or sintering.

Ordered mesopores carbons (OMCs) represent a distinguished class of nanomaterials with appealing structural characteristics such as high surface areas and uniform mesoporosity, which synthesis and applications have attracted much attention in recent years. The first synthesis was report by Ryoo et al. [13] in late 90´s - CMK-1 structure - and since then a considerable number of CMK-n (and other families) carbon materials have been prepared by nanocasting approaches [14, 15]. The good results obtained with CMK-n solids when tested as adsorbents [16], acid catalysts [17,18] and as supports for metal nanoparticles for hydrogenation reactions [19] or catalytic ammonia decomposition [20] have encouraged the persecution of studies to exploit the advantageous structural properties of such carbon materials in different catalytic processes.

In recent years, converting coal, natural gas and other sources into liquid fuels from various sources (coal, biomass, gas) via the Fisher-Tropsch (FT) process has lived a renewed interest. The production of high quality diesel-fuels involves the catalytic hydrocracking of the heaviest part of the FT hydrocarbons. On the other hand, the waxes produced in the FT unit can be upgraded to lubricant bases oil through catalytic

93 dewaxing [21]. This process consists on the removal of long-chain *n*-paraffins in order
94 to obtain a product with good cold-flow properties through the isomerization of
95 *n*-paraffins to branched iso-paraffins, through the so-called "isodewaxing" process [22,
96 23]. This method has considerable advantages against the classic removal of normal
97 paraffins by solvent extraction or by selective cracking.

98 The hydroisomerization of *n*-paraffins is commonly carried out over bifunctional
99 catalysts, with a hydrogenation/dehydrogenation function performed by a noble metal
100 (Pt or Pd) and acid sites for skeletal isomerization reaction involving carbenium ions
101 [24]. A review on the suitable catalysts properties for this reaction has been reported by
102 Deldari [25]. Among most important physicochemical features, ideal catalysts should
103 exhibit: a proper balance between the acid and metallic function, high dispersion of the
104 metal on the catalyst surface, medium pore size, mild acidity and strength distribution of
105 acid sites [25]. Besides the properties of the metal catalytically active phase, the nature
106 of the support is also relevant and characteristics concerning the average pore size, pore
107 opening, surface area and acidity of the supports have been reported to have important
108 effects on the performance of the bifunctional catalyst. For instance, the pore opening of
109 the support can control the selectivity of the catalytic reaction (if the pore opening is
110 small enough, the formation of *n*-paraffins over isoparafins is favored due to restricted
111 access to acidic sites). In brief, catalysts that have a high degree of hydrogenation
112 activity and a low degree of acidity are best for maximizing hydroisomerization versus
113 hydrocracking.

114 Bifunctional catalysts containing a noble metal (Pt or Pd) on a medium-pore
115 unidirectional molecular sieve such as SAPO-11 have shown a high
116 isomerisation/cracking ratio, with a high proportion of monobranched molecules within

117 the isomerised products [26]. Other molecular sieves such as ZSM-12, MOR, Y and
118 BEA zeolites have shown elevated conversions accompanied by high hydrocracking
119 yields due to the high acidity of these materials; mesoporous materials like MCM-41
120 have also shown good performance in hydroisomerization of long-chain *n*-paraffins
121 [27].

122 In this work we have explored the potentialities of porous carbon materials as
123 supports in the design and performance of Pt/carbon bifunctional catalysts for the
124 hydroisomerization of long chain *n*-alkanes. Despite the advantageous structural
125 properties of carbon materials, their application in this particular catalytic reaction has
126 not been reported so far. This is, to our best knowledge, the first reported study
127 exploiting the use of porous carbon materials for this catalytic reaction.

128

129 **Experimental**

130 1.1 Preparation of catalysts

131 The mesostructured silica SBA-15 was used as inorganic template for the synthesis of
132 the ordered mesoporous carbon CMK-3. The SBA-15 scaffold was prepared in a two-
133 step pathway using tetraethyl orthosilicate (TEOS, Aldrich) as the silica source and a
134 non-ionic surfactant ($(EO)_{20}(PO)_{70}(EO)_{20}$, Aldrich) following the procedure described
135 elsewhere [28]. Briefly, about 4.0 g of co-polymer $(EO)_{20}(PO)_{70}(EO)_{20}$ was dissolved in
136 126.05 cm^3 of 1.6 M HCl solution, and then ca. 9.1 cm^3 of TEOS was added under
137 constant stirring. The obtained solution was heated at 35 ºC for 24 h and allowed to age
138 at 100 ºC for 24 h. The white precipitate was filtered, dried and calcined at 550 ºC for
139 5 h with a heating rate of 1 ºC min^{-1}.

140 Sample CMK-3 was synthesized by nanocasting of the SBA-15 template using
141 sucrose as carbon precursor following the method described by S. Jun et al. [29]. In
142 short, about 1.25 g of sucrose (Sigma, 99.5%) was dissolved in 5.1 cm^3 H_2SO_4 solution
143 (0.14 g concentrated H_2SO_4 - José Manuel Gomes dos Santos, 95-97%- dissolved in 5
144 cm^3 of H_2O) and mixed to ca. 1.0 g of SBA-15 under stirring. The slurry was heated in
145 an oven to 100 ºC for 6 h and subsequently at 160 ºC for 6 h. The brownish powder
146 corresponding to the sucrose/silica composite was again impregnated with sucrose (i.e.,
147 0.8 g sucrose, 0.09 g concentrated H_2SO_4 and 5 cm^3 H_2O) and heated as indicated
148 before. The resulting black powder was then carbonized under vacuum at 875 ºC for 1 h
149 (heating rate 10 ºC min^{-1}). Removal of the silica template was carried out using HF
150 (48% solution, Sigma-Aldrich) at room temperature, followed by repeated washing in
151 distilled water until neutral pH was reached. The obtained carbon sample (CMK-3) was
152 dried at 95 ºC and stored in a dessicator until use.

153 The other carbon material used was a commercial carbon supplied by NORIT
154 (GL-50) was also used. To increase the content of oxygen surface complexes the sample
155 was submitted to a wet oxidation treatment using concentrated HNO_3 (i.e., 21 and 65
156 wt.%) at 100 ºC for 30 min. (ratio 1 g carbon/10 cm^3 HNO_3 solution). The oxidized
157 samples were thoroughly washed with water until no nitrates were detected. The
158 obtained samples will be labelled as GL-50(65) and GL-50(21).

159 The metal function was introduced on the carbon samples using the impregnation
160 method described by Coloma et al. [12], using $Pt(NH_3)_4Cl_2.xH_2O$ aqueous solution in
161 concentration needed to obtain a content of about 1% Pt (wt. %). The metal solution
162 was added to overnight dried carbon at 100 ºC and the stirring was maintained for 20 h
163 (ca. adsorption equilibrium as determined by kinetic measurements). After

164 equilibration, the remaining solution was removed and the sample dried. Before the
165 characterization and catalytic assays the samples were submitted to a two-stage protocol
166 to assure a good metal dispersion: (i) calcination under N_2 flow of 12 L h^{-1} g^{-1} at 400 ºC
167 for 2 h to allow the decomposition of the Pt precursor; (ii) reduction in H_2 flow of
168 6 L $h^{-1}g^{-1}$ at 400 ºC for 3 h in order to obtain the samples with the metal in the neutral
169 state.

170 1.2 Characterization

171 Textural characterization of the solids was carried out by means of gas adsorption.
172 N_2 adsorption isotherms at -196 ºC were recorded in an automatic apparatus
173 Micromeritics ASAP 2010, and used to evaluate total pore volumes, surface areas and
174 pore size distributions. Micropore volumes, V_{micro}, were obtained from *t*-method using
175 the Harkins-Jura equation [30], and mesopore volumes V_{meso}, were calculated by
176 subtracting V_{micro} from the amount adsorbed at $p/p^0 \approx 0.95$ [30]. The pore size
177 distribution (PSD) curves were obtained using the DFT methodology. Furthermore,
178 characterization of the microporosity was complemented by CO_2 adsorption isotherms
179 at 0 ºC, determined in a conventional volumetric apparatus equipped with an MKS-
180 Baratron (310BHS-1000) pressure transducer (0-133 kPa). The volume of narrow
181 micropores, V_{DRCO2}, was obtained from the Dubinin-Radushkevich equation [30].
182 Before the isotherms acquisition the samples (≈ 50 mg) were outgassed for 7 h at 120 ºC
183 under vacuum better than 10^{-2} Pa.

184 The surface chemistry of the carbon materials was characterized determining the
185 point of zero charge (pH_{PZC}) by the mass titration procedure [31]. Briefly, amounts of
186 the carbon material were dispersed in the suitable volume of ultrapure Milli-Q water

187 (typical carbon/water ratio are 4, 6, 8 and 10 wt.%), bubbled and sealed under N_2 in
188 glass vials. The slurries were stirred for at least 24 h at room temperature, and the pH
189 was measured using a glass electrode (SympHony SP70P VWR pH meter). The pH_{PZC}
190 value was estimated from the plateau of the curve pH *versus* solid weight fraction.

191 The surface oxygen groups incorporated upon oxidation of the carbon were identified
192 by temperature programmed desorption (TPD) using an Autochem II analyzer coupled
193 to an Omnistar mass detector in argon atmosphere. The amount of CO and CO_2 evolved
194 during the TPD experiments were quantified and linked to the nature of the
195 O-containing surface complexes in the carbons.

196 The amount of Pt incorporated in the carbon supports was determined from elemental
197 analysis, using inductively coupled plasma-optical emission spectrometer (ICP-OES)
198 Perkin Elmer Optima 2000 DV (λ = 265-945 nm). The analyses were performed at
199 'Laboratório de Análises', IST, Lisboa (Portugal).

200 Pt dispersion was evaluated by Transmission Electron Microscopy (TEM, Hitachi
201 H-8100 apparatus operating at 200 kV) and H_2 pulse chemisorption at 25 ºC
202 (Micromeritics ASAP 2900 unit equipped with a TCD detector). Prior to pulse
203 chemisorption experiments, all samples were reduced under H_2/Ar flow (50 cm^3/min)
204 for 1 h at 350 ºC. For each pulse chemisorption analysis, about 40-50 mg of sample
205 were treated with an Ar flow of 50 cm^3/min and pulses of 0.05 cm^3 (10% H_2 in Ar) until
206 saturation of the catalysts. To calculate metal dispersion, adsorption stoichiometry of
207 H/Pt = 1 [32] was assumed.
208
209

210 1.3 Catalytic tests

211 The catalytic tests were performed in flow reactors under a total pressure of 1 bar.
212 Toluene hydrogenation was used as a model reaction to characterize the metal sites
213 dispersed in the bifunctional catalyst at 110 ºC, using H_2/toluene molar ratio of 45 with
214 toluene diluted in *n*-hexane (1:5 molar ratio) and a space velocity of 100 h^{-1}, according
215 to the experimental procedure reported by Chupin et al. [33]. To obtain an accurate
216 value of the initial activity a multiple loop valve was used to allow collecting the reactor
217 effluent at very short time-on-stream. Although hydrogenation is a very exothermic
218 reaction, under the chosen operating conditions, only a small temperature increase
219 (lower than 5 ºC) was detected. The reaction products were analysed on-line by gas
220 chromatography using a Perkin Elmer Auto-System equipped with a flame ionisation
221 detector and a capillary column PONA.

222 *n*-Decane hydroisomerization was performed using a flow of 3 L h^{-1}, molar ratio
223 H_2/*n*-C_{10} of 14 and space velocity of 6.6 h^{-1}. The conversion was changed by varying
224 the reaction temperature from 280 to 350 ºC. The products were analysed on-line with a
225 gas chromatograph Hewlett-Packard 6890 series equipped with a flame ionisation
226 detector and a capillary column CP-Sil5.

227

228

229

230

231

2. Results and discussion

2.1 Supports characterization

The ash content of the sample CMK-3 was determined to check the efficiency of the silica scaffold removal step, as indicated in [2]. Briefly, the carbon matrix was burnt out and the mass balance was determined afterwards. The result obtained (ash content ca. 0.2 %) showed that a complete mineralization of the inorganic scaffold was achieved.

The results of nitrogen adsorption and TEM characterization of sample CMK-3 were presented and detailed discussed elsewhere [16]. In brief, the N_2 adsorption-desorption isotherm follows a typical type IV shape with hysteresis, according to IUPAC classification [34], revealing the mesoporous nature of the material. This is also evidenced in the textural parameters displayed in Table 1. The mesopore-size distribution is characterized by an intense and relatively narrow peak centered at pore-size diameter about 4 nm and a smaller peak around 8 nm pore size. The occurrence of all such pore sizes was also identified from TEM images where the 2D hexagonal structure of CMK-3 was clearly seen [16]. The images show that the material is formed by non-uniform hexagonal carbon rods, with average dimensions of about 7 nm × 8.5 nm. Some microporosity could also be disclosed, arising from slit shape pores between adjacent rods (pores around 1-2 nm). The largest pore volume (resulting from pores around 4 nm) results from the intersection of slits. Some irregularities in channel width were also noted in the TEM images. This was attributed to an incomplete filling of SBA-15 meso tunnels with carbon precursor, and also from the presence of a fraction of nonlinear channels in the SBA-15.

254 On the other hand, carbon GL-50 showed, as type I/IV isotherm (Figure 1),
255 characteristic of microporous materials with an important mesoporous network. To
256 assess the porosity evolution upon oxidation and Pt deposition the isotherms were
257 analyzed by different methods. The values quoted in Table 1 reveal that the oxidation
258 treatment brought about slight changes in the textural characteristics of this material.
259 The use of a concentrated HNO_3 solution (i.e., 65 wt.%) lead to a fall in the V_{meso}
260 whereas the V_{micro} remained rather unchanged; when less concentrated acid solution was
261 used a slight increase in the microporosity accessible to N_2 was observed. Such slight
262 increase in the surface area and V_{micro} upon oxidation at mild conditions is not the
263 expected trend commonly reported for oxidation of carbon samples, which is usually
264 associated to a drop in the specific surface area due to the destruction of some thin pore
265 walls and/or pore blocking by the fixation of surface oxygen groups at the pore
266 entrances [3, 35, 36].

267 Fig.1 and Table 1

268

269 As the major textural changes upon oxidation are expected to occur in the
270 micropore domain, the characterization of the samples by CO_2 adsorption was of
271 fundamental importance to account for the narrow microporosity of the samples (pore
272 width below about 0.7 nm) [37]. The increase in the CO_2 adsorption capacity upon
273 oxidation indicates a higher volume of narrow micropores, V_{DRCO2} (Table 1), as opposed
274 to the above-mentioned trend obtained from N_2 adsorption data. It must also be noted
275 that although in all cases $V_{DRN2} > V_{DRCO2}$ (characteristic of samples with a wide
276 microporosity), the difference between both parameters became larger with the

277 oxidation (accounting for ca. 50% in the case of sample GL-50(65)), confirming the
278 narrowing of the microporosity. The micropore size distributions, displayed in Fig. 2,
279 were assessed fitting the experimental CO_2 adsorption isotherms to the equation (1)
280 according to the method described by Pinto et al. [38]

281 $$w(A) = \sum_{i=1}^{m} w_{0i} exp\left[-\left(\frac{A}{\beta E_{0i}}\right)\right]^2 \quad (1)$$

282 where, w is the adsorbed volume, A is the adsorption potential ($A = -RT\ln(p/p^0)$, β
283 is the affinity coefficient (β = 0.36 for CO_2) and E_0 is the characteristic energy) that
284 depends on the porous solid and is related with the micropore width L in activated
285 carbons by

286 $$L(nm) = 10.8 \text{ nm kJ mol}^{-1} / (E_0 - 11.4 \text{ kJ mol}^{-1}) \quad (2)$$

287 This relation was recently confirmed comparison the adsorption with other experimental
288 techniques [39, 40]

289 These results allow a more detailed analysis of the oxidation treatments effect on
290 the microporosity modification. Oxidation in 21% HNO_3 solution results in a slight shift
291 of the maximum towards larger widths, along with a broadening of the distribution. This
292 is in agreement with the slight increase in the micropore volume accessible to N_2
293 molecules previously mentioned (Table 1) and suggests that mild oxidation has a
294 leaching effect that unblocks some micropores and/or promote the destruction of pore
295 walls increasing, either way, the volume accessible to the N_2 molecules. On the other
296 hand, oxidation in more concentrated acid solution leads to the opposite trend (the
297 displacement of the maximum towards smaller pore dimensions along with an increase

298 larger micropores) which suggests a more pronounced blocking effect of the pore
299 mouths by the incorporation of the oxygen functional groups.

Fig. 2

300 The oxidation treatment also had an accentuated effect on the surface chemistry of
301 the samples. The quantification of the thermodesorbed species by TPD-MS indicates
302 that, as expected, the amounts of CO and CO_2 (Table 2) evolved from the oxidised
303 carbons significantly increased after nitric oxidation [41]. The ratio CO/CO_2
304 considerably decreased upon the treatment which, according to the literature [42], is
305 related to the increase in carboxylic acid groups. These data is in good agreement with
306 the strong acid character of the oxidized samples, as it is inferred from the pH_{PZC} values
307 (Table 2), compared to the basic nature of the pristine carbon GL-50. The total oxygen
308 content calculated from the TPD assays shows a large increase in the oxygen content for
309 the most severe oxidation conditions.

310 Table 2

311

312 3.2 Characterization of bifunctional catalysts

313 The textural parameters of Pt supported carbons are presented in Table 1. In the case
314 of the catalysts obtained from GL-50 based samples the incorporation of the metal
315 function had no significant effect on the textural properties of the samples (Figure 1).
316 Conversely the preparation of sample Pt/CMK-3 was followed by an important decrease
317 of the mesopore volume. However, it is interesting to point out that the pore size
318 distribution curves (Figure 3) obtained using the DFT methodology revealed that no

319 displacement on the maximum position was observed despite the fall in the mesopore
320 volume. This suggests that a pore blocking occurred upon immobilization of the Pt
321 nanoparticles, rather than a shrinkage of the average pore sizes motivated by a partial
322 pore plugging.

323 Fig. 3

324 The metal function of the Pt loaded carbons was characterized by TEM, H_2
325 chemisorption and by the model reaction of toluene hydrogenation. Figure 4 shows
326 TEM images for all studied Pt-loaded catalysts.

327 Fig. 4

328 Figure 4 (A) shows a broad size distribution of Pt particles when CMK-3 carbon
329 was used as support. The largest and darkest spots can be attributed to Pt clusters
330 located on the external surface of Pt/CMK-3 sample. Other less clear and smaller spots
331 can be ascribed to Pt particles located inside the mesopores. Such a heterogeneous
332 distribution of metallic particles of different sizes led us to postulate that smaller Pt
333 particles are located inside the pores in the carbon matrix, while the largest particles
334 would be located outside. For the microporous commercial carbon, it is notorious that
335 the oxidation treatments lead to a more homogeneous dispersion with Pt particles of
336 uniform sizes. The visualization of TEM images also suggests that the majority of Pt
337 introduced is located at outer surface of the carbon with only a small amount inside the
338 pores. This was particularly visible for Pt/GL-50(21) sample and less notorious for
339 Pt/GL-50(65); based on the similar textural features of the carbons (Table 1), it can thus
340 be inferred that the surface modifications as a consequence of the oxidation determine
341 the location of Pt particles. The enhanced metal dispersion on carbon materials with
342 high densities of oxygen surface functionalities has been previously reported, and

343 explained due to the capacity of the surface groups to act as anchoring sites for the
344 metallic function [43]. However, based on these results it seems that on mild oxidation
345 (21 % HNO_3) most of the surface functional groups would be mainly located near the
346 outer surface of the carbon particles; in contrast, a more homogeneously distribution in
347 the carbon matrix would be obtained when oxidizing with 65% HNO_3. It has to be
348 mention that the use of highly concentrate HNO_3 is not commonly reported in the
349 literature [3, 35, 42] although from our results we can conclude that the surface
350 chemistry modification lead to an optimized bifunctional catalyst with small and
351 homogeneously distributed Pt particles over both outer and inner surfaces.

352 The results obtained by H_2 chemisorption assays are displayed in Table 3 show a
353 low metal dispersion for Pt/CMK-3, in good agreement with TEM images. The metallic
354 dispersion increased for the oxidized microporous carbons which present values about 5
355 to 6 times higher. Although the same effect has been described by other authors [43,
356 44], our results suggest that beyond the positive effect of oxidation on favouring the
357 metal dispersion on the carbon matrix, the concentration of the oxidation agent strongly
358 affects the location of the metallic particles within the support.

359 From the dispersion values, D_{H2}, obtained by H_2 chemisorption the mean particle
360 size, d_{H2}, was evaluated assuming that one H atom was chemisorbed by one surface Pt
361 atom and that $d_{H2}=1.08/D_{H2}$ [24]. The results are reported in Table 3 and show that the
362 mean Pt particle size on GL-50 oxidized supports are similar and smaller (one order of
363 magnitude) than that observed for Pt/CMK-3. These values are in accordance with the
364 particle size range estimated from the analysis of TEM images, Δd_{TEM}, revealing that
365 the experimental conditions used in reduction led to a complete transformation of Pt(II)
366 into Pt(0). The large Pt nanoparticles observed for Pt/CMK-3 are most likely due to the

367 mesopore nature of this material that would allow the formation of large Pt clusters
368 inside the mesopores; this is in accordance with the mesopore volume drop observed
369 upon the Pt incorporation (Table 1). Large Pt nanoparticles of a few mesopores width
370 were also observed for the pristine GL-50 carbon. Given its porous features, this effect
371 could also be attributed to the mesopores present in this carbon. However, it is
372 interesting to remark that smaller metallic particles (Δd_{TEM}) were obtained in both
373 oxidized samples, which textural features were similar to those of the pristine GL50
374 carbon. Consequently, for these samples the smaller size of the metallic particles cannot
375 be attributed to the texture of the carbon support. Differences must be explained thus in
376 terms of the surface chemistry, confirming the outstanding role of the oxygen
377 functionalities on the dispersion, location and average size of the metallic particles.

378 Table 3

379 The catalytic activity in hydrogenation of benzenic hydrocarbons (benzene or less
380 toxic toluene) is often used to characterize metal dispersion, as it has been demonstrated
381 [45] that the hydrogenating activity of a given catalysts is proportional to the
382 concentration of accessible metal sites, being insensitive to matrix structure. Under the
383 chosen experimental conditions toluene hydrogenation was totally selective to
384 methylcyclohexane. Figure 5 shows the evolution of hydrogenating activity with time-
385 on-stream (deactivation curves). Initial hydrogenating activities normalized by the
386 amount of Pt introduced are displayed in Table 3.

387 Fig.5

388 The deactivation curves show a common behaviour for Pt/CMK-3 and Pt/GL-50
389 samples, with a high activity in the first instants of the reaction followed by a sharp

390 decrease and a low activity plateau. The initial hydrogenating activity, taken after 1 min
391 time-on-stream, shows a higher value for Pt/CMK-3 compared to the series of
392 microporous carbon-supported catalysts (Pt/GL-50 and its two oxidized counterparts).
393 This result was rather unexpected since Pt/CMK-3 presents the lowest metal dispersion,
394 with large Pt particles located mainly at the carbon external surface (Table 3 and Figure
395 4). The most plausible explanation for this behaviour could be linked to the role of the
396 mesoporosity on the kinetics of the hydrogenation reactions, which would increase the
397 circulation of reactant molecules and hence the initial hydrogenation activity.
398 Analogously, the predominant microporous character of GL-50 carbons limits the
399 diffusion of species inside the pores, leading to slightly lower hydrogenating activities
400 compared to CMK-3 (despite the low metal dispersion).

401 On the other hand, the effect of oxidation of the carbon support on the initial
402 hydrogenating activity is displayed on Table 3. For sample Pt/GL50(65), the initial
403 hydrogenating activity was more than 10 times higher than the one presented for Pt/GL-
404 50(21), and about 32 times higher than that of non-oxidized pristine carbon.
405 Considering that Pt contents and textural features are similar in the three samples, such
406 large differences in the initial hydrogenation activity can be ascribed to Pt dispersion
407 and location and also to the access to the metallic sites. In this sense, TEM images
408 indicated that dispersion of the Pt particles was significantly improved upon oxidation
409 of the carbon support, along with a more homogenous distribution of the particles
410 within the carbon matrix (both in the internal and external surface). Moreover the
411 location of the metallic particles is also favourably located mainly at the external
412 surface.

These results corroborate that the catalytic activity does not only depend on metal dispersion but it also relies on other effects like the location of the metal particles that influence the reactant accessibility to the metal sites [44].

3.3 Hydroisomerization of *n*-decane

The hydroisomerization of long chain *n*-alkanes was performed using *n*-decane as a model molecule, since it has a number of carbon atoms sufficiently large to simulate the most important types of mechanisms that occur with long chain *n*-alkanes. Figure 6 shows the evolution of total conversion of *n*-decane with the reaction temperature for Pt/CMK-3 and Pt/GL-50(21) and (65) samples. Pt/GL-50 sample was not further considered for this catalytic reaction due to its extremely low hydrogenation activity (Table 3). In order to account possible initial deactivation phenomena each data point was acquired after 20 min time-on-stream.

Fig. 6

All three explored catalysts followed a common predicted pattern, with increased conversion with rising the reaction temperature regardless the nature of the carbon support or the dispersion and location of the metallic function. Conversions ranged from 4% at 280ºC to 8-10% at 350ºC, for the three samples, with a slightly higher value for sample Pt/CMK-3 when the reaction was carried out at 350 ºC. This slighth difference might be related with the higher hydrogenating activity of this sample along with the faster accessibility due to the mesoporous character of CMK-3 carbon.

434 The pattern for product distribution was also common to all three catalysts, with
435 *n*-decane converted to mono (M) and dibranched (D) isomers and cracking products (C)
436 (for hydrocarbons with less than 10 carbon atoms). The product distribution for
437 Pt/CMK-3 sample is shown in Figure 7 as an example. The isomerization products,
438 mainly monobranched isomers are the main reaction products, with more than 75%
439 selectivity at low temperature that decreases to about 40% at the highest temperature.
440 The cracking products increased with the conversion and temperature, which indicates
441 that skeletal isomerization of *n*-decane to monobranched isoalkanes prevails at low
442 conversion [25] whereas dominancy of cracking reactions occurs at high temperatures.
443 The analysis of cracking products shows a broad distribution of compounds, which
444 indicates that the reaction intermediates undergo oligomerization reactions before
445 cracking, originating fragments with a number of carbon atoms ranging from two to
446 nine (C_2-C_9).

447 Also, as monobranched paraffins are less susceptible to cracking than
448 multibranched paraffins, it seems that monobranched isomers are favored at low
449 conversion.

450 Fig.7

451 Figure 8 displays the ratio between the sum of isomerization (I=M+D) and
452 cracking products at similar conversion of about 4% at 280ºC for the threes studied
453 catalysts. Although the Isomerization/Cracking (I/C) ratio was of the same order of
454 magnitude for all samples, the lowest value was obtained for Pt/CMK-3 sample which
455 indicates the predominance of cracking reactions event at low conversion. On the other
456 hand both oxidized carbon, and particularly carbon Pt/GL-50(21), present the high I/C

457 ratios pointing out the predominance of fast isomerization reactions over hydrocracking.
458 These difference must be explained in terms of the textural features of the catalyst; the
459 larger pore diameter of Pt/CMK-3 would allows the formation of bulky oligomers
460 before undergoing cracking reactions, whereas for the microporous carbon supports, the
461 isomerization kinetics would be favoured at the external surface where the majority of
462 metallic active sites are located.

463 Fig. 8

464 Figure 9 shows the ratio between monobranched and dibranched isomers (M/D)
465 at similar conversion of 4% and 280ºC. As envisaged, all bifunctional catalysts are able
466 to privilege the formation of monobranched isomers, which are the products of major
467 interest. The intrinsic acidity of Pt/CMK-3 catalyst allows this material to behave as a
468 bifunctional catalyst without further functionalization of the carbon surface.
469 Nevertheless the poor metal dispersion along with the mesoporous character of this
470 sample promotes the occurrence of more than one isomerization step on the acid sites
471 before reaching the hydrogenating sites, resulting on the lowest M/D ratio. Concerning
472 GL-50 based materials; both oxidized carbons display higher M/D ratios, particularly
473 Pt/GL-50(65). This is due to the combination of mild acidity and homogeneous metal
474 dispersion achieved for this catalyst as a consequence of the oxidation using
475 concentrated nitric acid. Further, the micropore size distribution of GL-50 carbon (see
476 Figure 2) is similar to the pore size of the typical industrial catalyst used for long chain
477 hydroisomerization reactions, SAPO-11 [25, 46].

478 The resulting bifunctional catalyst has an adequate ratio between acid and
479 metal sites that promotes the occurrence of one isomerization step on the

480 acid sites between dehydrogenation/hydrogenation steps on the metallic sites
481 [47, 48] resulting in the preferential formation of monobranched isomers, with
482 a catalytic behaviour identical to the one presented by Pt/SAPO-11 catalyst
483 assayed under the same experimental conditions.

484 Fig. 9

485

486 **3. Conclusions**

487 In the present work the potentialities of Pt/carbon based on two texturally different
488 materials - a mainly microporous carbon from NORIT (GL-50) and an ordered
489 mesoporous carbon (CMK-3) - were explored as bifunctional catalysts in
490 hydroisomerization of long chain *n*-paraffins, using *n*-decane as a model molecule:

491 To order to increase the surface acidity GL-50 sample was submitted to wet
492 oxidation with 21 and 65 % wt. HNO_3 solutions. These treatments had a pronounced
493 effect on the surface chemistry of the samples leading to the increase of the oxygenated
494 surface groups that were more homogenously dispersed in the carbon matrix when more
495 concentrated acid was used. These characteristics allowed the preparation of a
496 bifunctional catalyst with small and homogenously dispersed Pt particles over outer and
497 inner surfaces. On the contrary, when CMK-3 was used as support lower metal
498 dispersion was observed with large Pt particles both inside and outside pores. The high
499 hydrogenating activity of this sample was attributed to the mesopore nature of the
500 support that enhances the molecular traffic inside the pores.

In *n*-decane hydroisomerization all catalysts presented identical conversions and product distribution in the temperature range that was studied. However Pt/GL-50(65) privileges the formation of monobranched isomers, which are the most valuable products, when compared with Pt/GL-50(21) or even Pt/CMK-3 materials, tested in the same conditions. For Pt/GL50(65) sample, optimized acidity and metal dispersion was attained along with adequate porosity making this material suitable to work as a bifunctional catalysts in hydroisomerization of long chain n-alkanes, presenting a catalytic behaviour similar to the commercial catalyst Pt/SAPO-11.

The catalytic application explored in this study is not common for carbon supported bifunctional catalysts, however it should be mentioned that carbon materials have some advantages when compared with zeolites or related materials since they can be synthesized from wastes allowing the valorization of industrial and agricultural sub-products. Further, upon catalysts deactivation the recycling of precious metals (from hydrogenating function) is especially facilitated since it only requires the burning of the support.

Acknowledgements

This work was financially supported by Fundação para a Ciência e Tecnologia (FCT) through Projects PTDC/CTM/65718/2006 Pest-OE/QUI/UI0612/2011 (Strategic Project) .and MINECO (CTM2011/23378). Authors wish to thank the collaboration of SALMON & Cia for supplying GL-50 carbon from NORIT.

524 **References**

525 [1] A.P. Carvalho, M. Gomes, A.S. Mestre, J. Pires, M. Brotas de Carvalho, Carbon 42
526 (2004) 672–674.

527 [2] A.S. Mestre, J. Pires, J.M.F. Nogueira, A.P. Carvalho, Carbon 45 (2007) 1979-1988.

528 [3] C.O. Ania, J.G. Pelayo, T.J. Bandosz, Adsorption 17 (2011) 421-429.

529 [4] H. Marsh, F. Rodriguez-Reinoso, Activated Carbon, Elsevier, Oxford, 2006

530 [5] A.S. Bexiga, M. Proença, M. Andrade, A.S. Mestre, M. Pinto, I. Matos, I. M.
531 Fonseca, A.P. Carvalho, Bioresour. Technol. 102 (2011) 8253-8260.

532 [6] J. Hayashi, T. Horikawa, K. Muroyama, V.G. Gomes, Microp. Mesop.Mater. 55
533 (2002) 63-68.

534 [7] F. Rodríguez-Reinoso, A. Sepúlveda-Escribano, H.S. Nalwa /Ed.), Handbook of
535 Surfaces and Interfaces of Materials, Vol. 5: Biomolecules, Biointerfaces and
536 Applcations, Academic Press, London, 2001, p.309-355.

537 [8] A.M. Fuente, G. Pulgar, F. González, C. Pesquera, C. Blanco, Appl. Catal. A: Gen.
538 208 (2001) 35-46.

539 [9] L. Li, S.H. Zhu, Z.F Yan, G.Q. Lu, L. Rintoul, Appl. Catal. A: Gen. 320 (2007) 166-
540 172.

541 [10] T. Reshetenko, L.A. Avdeeva, Z.R. Ismagilov, A.L. Chuvilin, V.B. Fenelonov,
542 Catal. Today, 102-103 (2005) 115-120.

543 [11] F. Alonso, P. Riente, F. Rodríguez-Reinoso, J. Ruiz-Martínez, A. Sepúlveda-
544 Escribano, M. Yus, Chem. Cat. Chem. 1 (2009) 75-77.

545 [12] F. Coloma, A. Sepúlveda-Escribano, J.L.G. Fierro, F. Rodriguez-Reinoso, Appl.
546 Catal. A: Gen.150 (1997) 165-183.

547 [13] R. Ryoo, S.H. Joo, S. Jun, J. Phys. Chem. B, 103 (1999) 7743-7746.

548 [14] B. Sakintuna, Y. Yürüm, Ind. Eng. Chem. Res., 44 (2005) 2893-2902.

549 [15] J. Lee, J. Kim, T. Hyeon, Adv. Mater., 18 (2006) 2073–2094.

550 [16] V.K. Saini, M. Andrade, M.L. Pinto, A.P. Carvalho, J. Pires, Sep. Purif. Technol.
551 75 (2010) 366-376.

552 [17] X. Wang, R. Liu, M.M. Waje, Z. Chen, Y. Yan, K.N. Bozhilov, P. Feng, Chem.
553 Mater. 19 (2007) 2395-2397.

554 [18] L. Peng, A. Philipparerts, X. Ke, J.V. Noyen, F. De Clippel, G.V. Tendeloo, P.A.
555 Jacobs, B.F. Sels, Catal. Today 150 (2010) 140-146.

556 [19] M. Boutros, G. Shirley, T. Onfroy, F. Launay, Appl. Catal. A: Gen. 394 (2011)
557 158-165.

558 [20] A.-H. Lu, J.-J. Nitz, M. Comotti, C. Weithenthaler, K. Schlichte, C.W. Lehmann,
559 O. Terasaki, F. Schüth, J. Am. Chem. Soc. 132 (2010) 14152-14162.

560 [21] C. Bouchy, G. Hastoy, E. Guillon, J.A. Martens, Oil Gas Sci. Technol. 64 (2009)
561 91-112.

562 [22] S.J. Miller, US Patent 4 859 311 to Chevron (1989)

563 [23] S.J. Miller, US Patent, 4 859 312 to Chevron (1989).

564 [24] J.L. Figueiredo, F. Ramôa Ribeiro, Catálise Heterogénea, 2nd Ed., Fundação
565 Calouste Gulbenkian, Lisboa, 2007.

566 [25] H. Deldari, Appl. Catal. A: Gen., 293 (2005) 1-10

567 [26] T. Blasco, A. Chica, A. Corma, W.J. Murphy, J. Agúndez-Rodriguez, J. Pérez-
568 Pariente, J. Catal. (2006) 153-161.

569 [27] K.-C. Park, S.-K. Ihm, Appl. Catal. A: Gen. 203 (2000) 201-209.

570 [28] M. Choi, F. Kleitz, D. Liu, H. Yoon Lee, W.S. Ahn, R. Ryoo, J. Amer. Chem. Soc.
571 127 (2005) 1924-1932

572 [29] S. Jun, S.H. Joo, R. Ryoo, M. Kruk, M. Jaroniec, Z. Liu, T. O. Ohsuna, Terasaki, J.
573 Amer. Chem. Soc. 122 (2000) 10712-10713.

574 [30] F. Rouquerol, J. Rouquerol, K.S.W. Sing, Adsorption by Powders and Porous,
575 Academic Press, London, 1999.

576 [31] J.S. Noh, J.A. Schwarz, J. Colloid Interface Sci. 130 (1989) 157-164.

577 [32] C. Pedrero, T. Waku, E. Iglesia, J. Catal. 233 (2004) 242-255.

578 [33] J. Chupin, N.S. Gnep, S. Lacombe, M. Guisnet, Appl. Catal. A: Gen. 206 (2001)
579 43-56.

580 [34] J. Rouquerol, D. Avnir, C.W. Fairbridge, D.H. Everett, J.H. Haynes, N. Pernicone,
581 J.D.F. Ramsay, K.S.W. Sing, K.K. Unger, Pure and Applied Chemistry 66 (1994) 1739-
582 1758.

583 [35] M. B. Dawidziuz, F. Carrasco-Marín, C. Moreno-Castilla, Carbon 47 (2009) 2679-
584 2687.

585 [36] B. Ruiz, I. Cabrita, A.S. Mestre, J.B. Parra, J. Pires, A.P. Carvalho, C.O. Ania,
586 Appl. Surf. Sci. 256 (2010) 5171-5175.

587 [37] D. Carzola-Amorós, J. Alcañiz-Monge, M.A. de la Casa-Lillo, A. Linares-Solano,
588 Langmuir 14 (1998) 4589-4596.

589 [38] M.L. Pinto, A.S. Mestre, A.P. Carvalho, J. Pires, Ind. Eng. Chem. Res. 49 (2010)
590 4726-4730.

591 [39] F. Stoeckli, A. Slasli, D. Hugi-Cleary, A. Guillot, Microp. Mesop.Mater. 51 (2002)
592 197-202.

593 [40] F. Stoeckli, A. Guillot, A. M. Slasli, D. Hugi-Cleary, Carbon 40 (2002) 383-388.

594 [41] T.J. Bandosz, C.O. Ania, in T.J. Bandosz (Ed.), Activated Carbon Surfaces in
595 Environmental Remediation, Vol.7, Elsevier Amsterdam, 2006, pp.159-229.

596 [42] J.L. Figueiredo, M.F.R. Pereira, M.M.A. Freitas, J.J.M. Órfão, Carbon 37 (1999)
597 1379-1389.

598 [43] E.E. Aksoylu, M.M. A. Freitas, M.F.R. Pereira, J.L. Figueiredo, Carbon (2001)
599 175-185.

600 [44] G.C. Torres, E.L. Jablonski, G.T. Baronetti, A.A. Castro, S.R. Miguel, O.A.
601 Scelza, M.D. Blanco, M.A, Peña Jiménez, J.L.G. Fierro, Appl. Catal. A: Gen. 161
602 (1997) 213-226.

603 [45] M. Boudart, J. Mol. Catal. 30 (1985) 27-38.

604 [46] R. Bértolo, A. Fernandes, F. Ribeiro, J.M. Silva, A. Martins, F.R. Ribeiro, React.
605 Kinet. Mech. Cat., 99 (2010) 183-191.

606 [47] F. Alvarez, F.R. Ribeiro, G. Perot, C. Thomaseau, M. Guisnet, J. Catal. 162 (1996)
607 179-189.

608 [48] M. Guisnet, F. Alvarez, G. Gianetto, G. Perot, Catal. Today 1 (1987) 415-433.

609 **Table 1.** Textural parameters of the supports and bifunctional catalysts.

610

Sample	A_{BET} (m^2g^{-1})	V_{micro} [a] (cm^3g^{-1})	V_{meso} [b] (cm^3g^{-1})	A_{ext} (m^2g^{-1})	V_{DRCO2} (cm^3g^{-1})
CMK-3[c]	1396	0.14	1.12	-	
GL-50	744	0.30	0.18	124	0.24
GL-50(21)	821	0.33	0.19	112	0.25
GL-50(65)	711	0.29	0.11	74	0.26
Pt/CMK-3	971	0.13	0.74	-	-
Pt/GL-50	714	0.28	0.16	113	-
Pt/GL-50(21)	770	0.31	0.15	113	-
Pt/GL-50(65)	712	0.30	0.13	94	-

611 [a] microporous volume determined by the *t*-method.

612 [b] $V_{meso}=V_{total}-V_{micro}$; V_{total} is the amount adsorbed at $p/p^0=0.95$.

613 [c] results from [16]

614

615 **Table 2**
616 Surface chemistry of the supports: pH_{PZC}, amounts of CO and CO_2 evolved in TPD
617 assays, ratio CO/CO_2, and total oxygen amount.
618

Sample	pH_{PZC}	CO μmol/g	CO_2 μmol/g	CO/CO_2	O_{TPD} (wt.%)
CMK-3[c]	4.7	1015	79	12.81	1.9
GL-50	11.9	1015	79	12.81	8.6
GL-50(21)	2.7	2799	1292	2.17	11.8
GL-50(65)	3.0	3702	1841	2.01	1.9

619

620 **Table 3**

621 Platinum contents, metal dispersion, D_{H2} and mean particle size, d_{H2}, from H_2
622 chemisorption, particle size range, Δd_{TEM}, estimated from TEM images, and initial
623 hydrogenating activities for toluene hydrogenation.
624

Sample	Pt content (wt.%)	D_{H2} (%)	d_{H2} (nm)	Δd_{TEM} (nm)	Initial activity (mol h^{-1} μmol_{Pt})
Pt/CMK-3	0.90	6.6	16.4	12-35	0.0716
Pt/GL-50	0.61	n.d.	n.d.	13-25	0.0021
Pt/GL-50(21)	0.89	36.0	3.0	2-6	0.0057
Pt/GL-50(65)	0.93	41.4	2.6	2-6	0.0677

625

626 **Fig.1.** Nitrogen adsorption-desorption isotherms for the indicated samples.

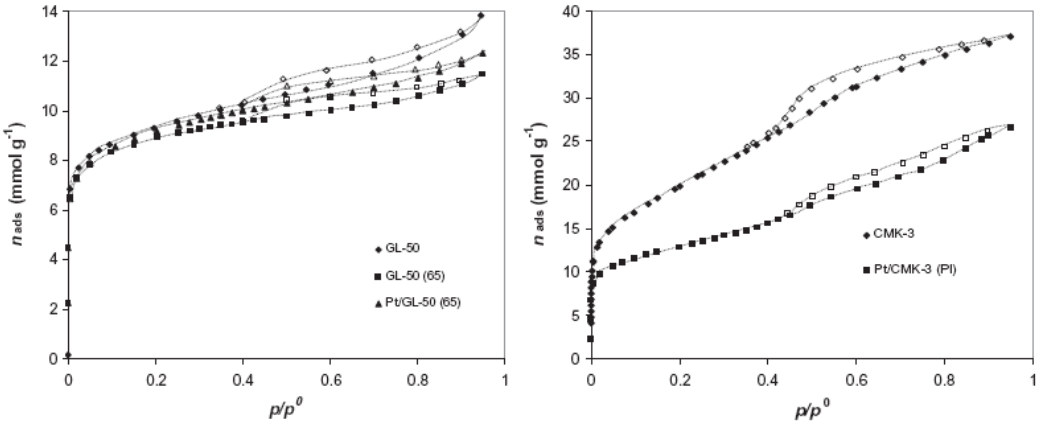

627

628

629 **Fig.2.** Micropore size distributions obtained by fitting Eq. (1) to the CO_2 adsorption
630 isotherms at 0 ºC, according to the method described by Pinto et al. [38] for the
631 indicated samples.

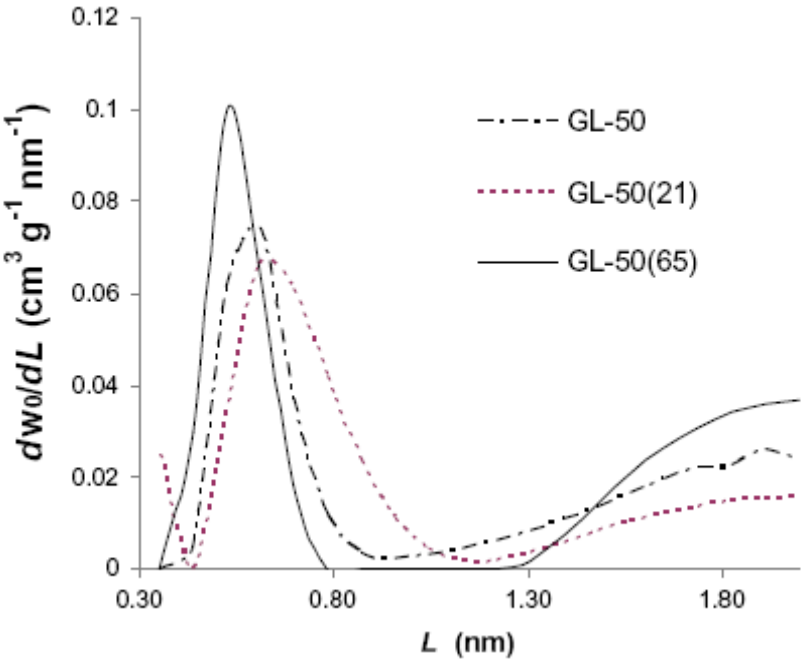

632

633 **Fig.3.** Mesopore size distribution obtained by DFT method to the N_2 adsorption

634 isotherms a -196 ºC for the indicated samples.

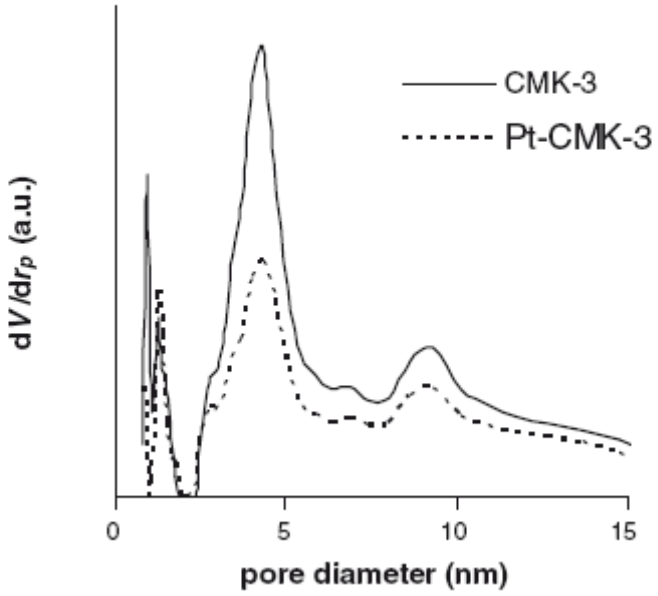

635

636 **Fig.4.** TEM images of Pt/CMK-3 (A), Pt/GL-50 (B), Pt/GL-50(25) (C) and Pt/GL-

637 50(65) (D).

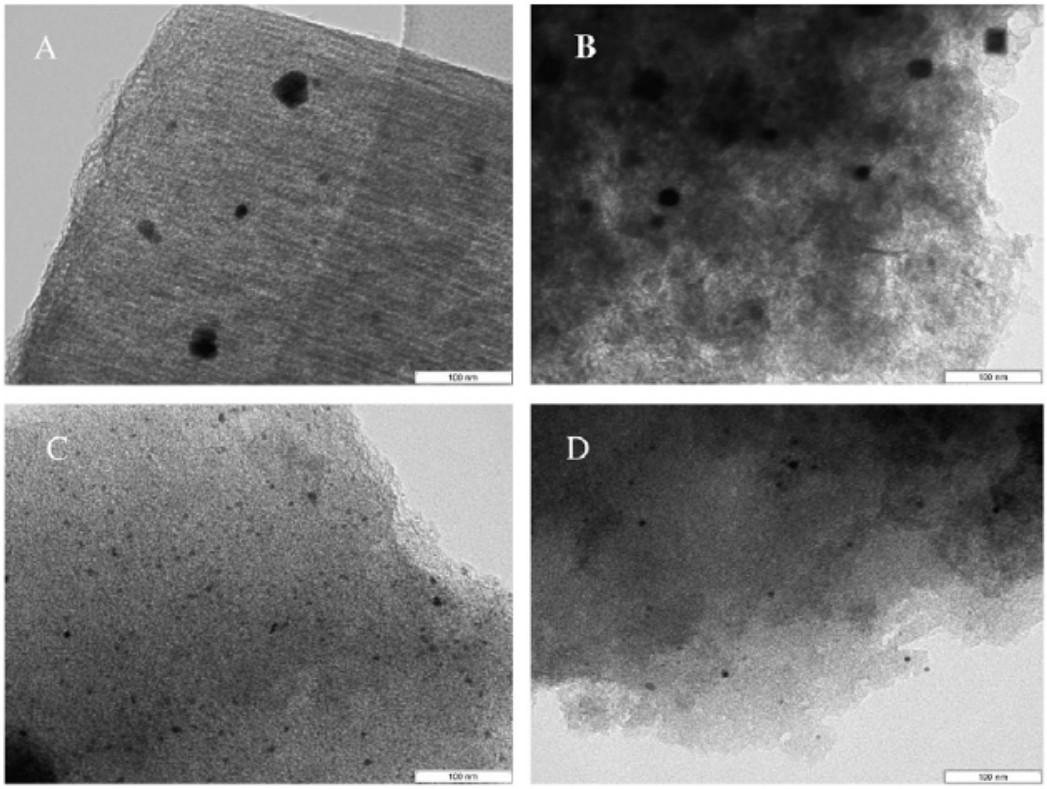

638

639 **Fig. 5.** Deactivation curves for toluene hydrogenation at 110 ºC.

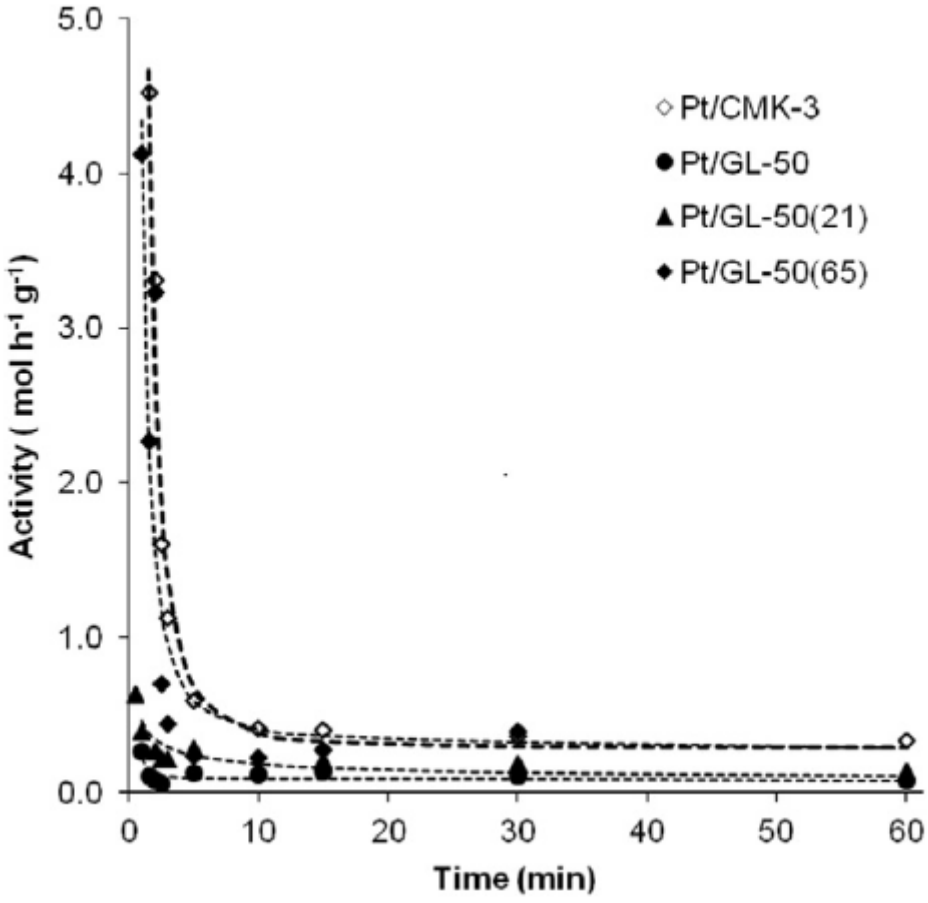

640

641 **Fig. 6.** Conversion as a function of reaction temperature for *n*-decane

642 hydroisomerization.

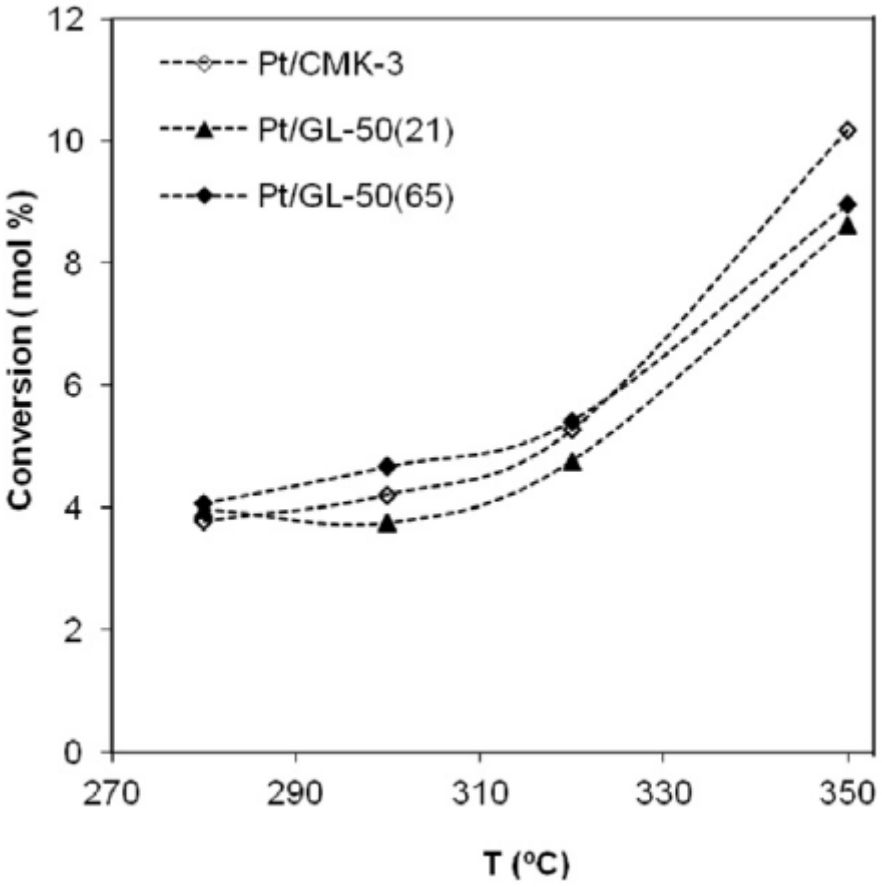

643

644 **Fig. 7.** Product families distribution for Pt/CMK-3 catalyst in *n*-decane
645 hydroisomerization.

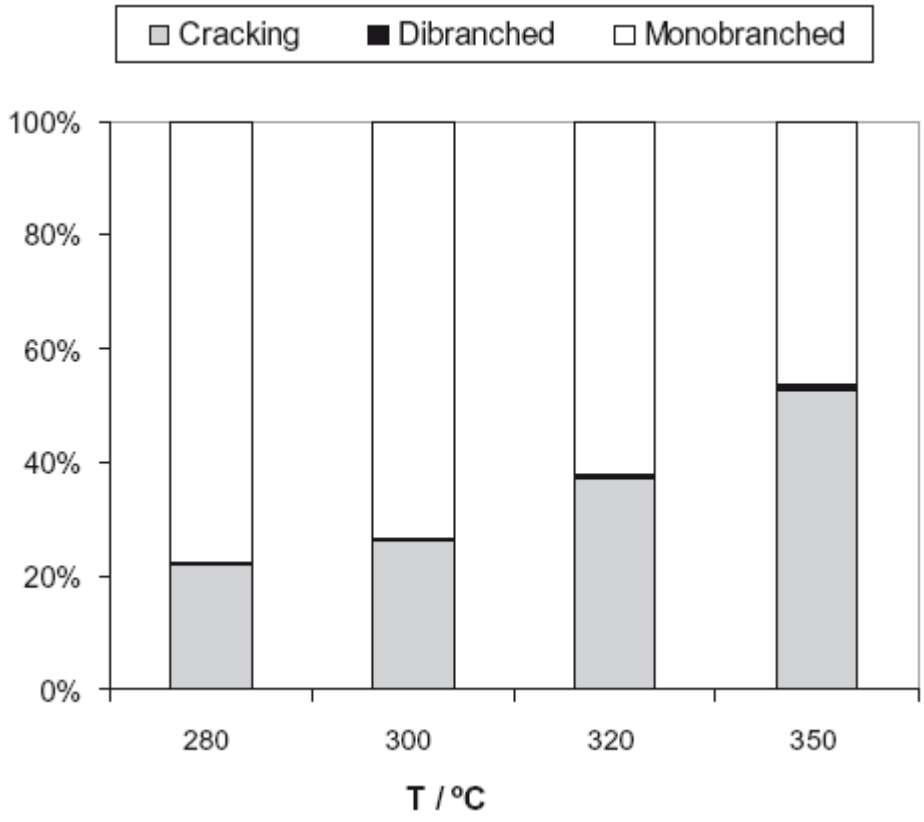

646

647 **Fig. 8.** Ratio between the sum of isomerization and cracking products for *n*-decane

648 hydroisomerization at 270ºC and similar conversion around 4 %.

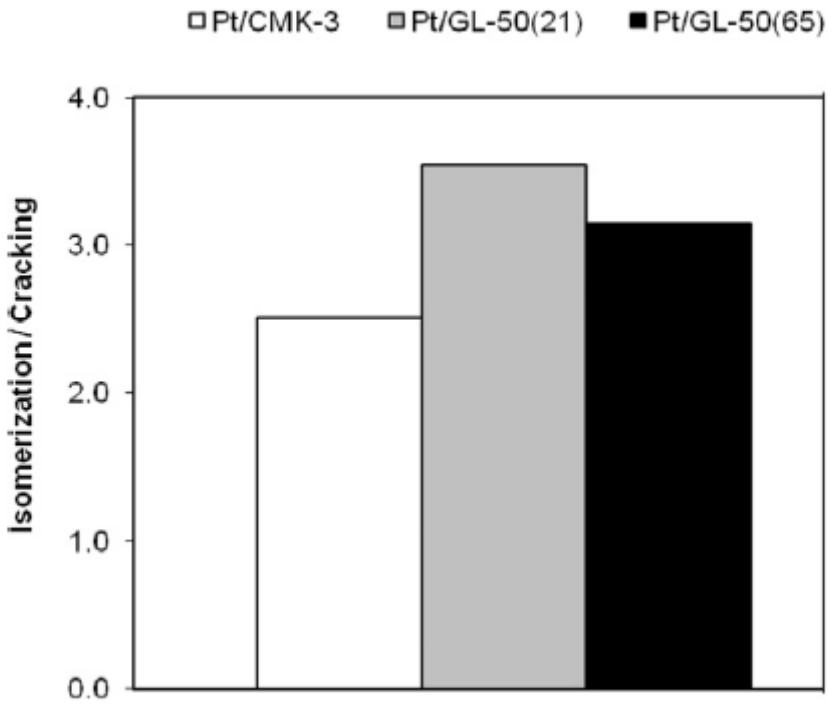

649

650 **Fig. 9.** Ratio between the sum of monobranched isomers and the sum of dibranched
651 ones for *n*-decane hydroisomerization at 270ºC and similar conversion around 4 %.

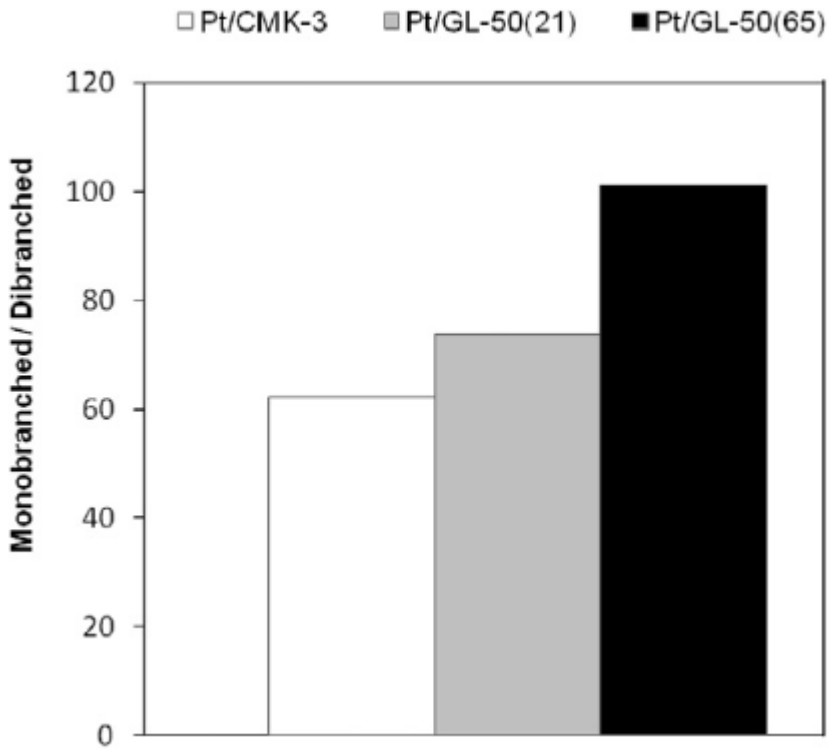

652